Parametrically Robust Identification Based Sensorless Control Approach for Doubly Fed Induction Generator

Anuprabha Ravindran Nair, *Graduate Student Member, IEEE*, Rojan Bhattarai, *Member, IEEE*, Michael Smith, *Member, IEEE*, and Sukumar Kamalasadan, *Senior Member, IEEE*

***Abstract*—This article proposes a modified adaptive control architecture for doubly fed induction generator DFIGs connected to the power grid that can be augmented with the existing conventional vector control of DFIG. The architecture uses online identification of the system transfer function using recursive least squares (RLS). An auto-regressive moving average system model is identified by the RLS algorithm. A minimum variance control architecture then defines an adaptive control law based on the identified model parameters for DFIG control by minimizing the difference of the system output from the model output. The control method nullifies the issues commonly experienced with conventional techniques (e.g., malfunctioning sensors, parameter variations) and ensures acceptable performance during variable grid operating conditions, where the conventional proportional-integral controller commonly fails. Several test cases are performed to analyze and validate the overall performance using real-time simulation for a 1.5 MW wind turbine system.**

***Index Terms*—Adaptive control, doubly fed induction generator (DFIG) control, renewable energy, sensorless control, system identification.**

I. Introduction

A WIND turbine doubly fed induction generator (DFIG) typically uses a back-to-back converter for controlling active and reactive power through the voltage and provides balanced power at the stator terminals [1], [2]. Currently, DFIG-based wind energy conversion systems (WECS) occupy approximately 50% of the wind energy market. These type 3 (DFIG) based WECS are popular, because of their comparatively smaller sized power converters, maximum power extraction capability through variable speed operation, ease in the machine controllability, and additional auxiliary services (e.g., providing grid voltage stability and frequency control). Several DFIG control topologies have been proposed and tested, out of which the most widely used method is vector control (VC) [3]. A conventional VC approach offers the potential for acceptable DFIG control performance, but is dependent on dq transformation and demands accurate knowledge of many parameters to properly tune the controller. However, the conventional VC approach with static controllers necessitates additional tuning to maintain acceptable performance as the operating condition varies [4], [5]. Also, the outer feedback loop in the VC approach relies on accurately measured real and reactive power and rotor currents (based on sensors) for the feedback loop.

Uncertainty in WECS operation (resulting from the unpredictable nature of wind, the load, and its effect on the robust operation of wind energy-based systems) has been discussed in detail [6]. This work mainly reviews the causes of failure for wind turbines and the importance of wind turbine condition monitoring to reduce the cost of unplanned downtime. Another area focuses on the wind turbine failure rate and the need for proper cost-effective maintenance procedures to support robust performance. This work analyzes the failure rates of onshore geared and direct driven wind turbines. Understood from this work, failures caused by sensors and communication issues lead to significant economic losses, because of power losses with the increased penetration of wind-based sources [7]. In [8] and [9], rotor currents are estimated based on stator voltage and power measurements using state feedback observers. The main objective of this approach is to reduce the dependency on rotor current sensors, but these techniques rely on prior knowledge of the parameters defining the system (e.g., stator and rotor resistances and inductances). Recent methods that use the estimated rotor currents as feedback signals in VC are proposed that improve the operational reliability of a DFIG over a wide range [10]–[13]. A modified current controller-based DFIG system with superior operational reliability has been discussed in literature [14], [15]. Most of these control approaches are senor based, so sensor

Manuscript received April 17, 2020; revised August 22, 2020; accepted October 2, 2020. Date of publication November 3, 2020; date of current version December 31, 2020. Paper 2020-IACC-0685.R1, presented at the 2019 IEEE Industry Applications Society Annual Meeting, Baltimore, MD, USA, Sep. 29 to Oct. 3, and approved for publication in the IEEE Transactions on Industry Applications by the Industrial Applications and Controls Committee of the IEEE Industry Applications Society. This work was supported by the National Science Foundation under Grant ECCS-1810174 awarded to the last author. *(Corresponding author: Sukumar Kamalasadan.)*

Anuprabha Ravindran Nair, Michael Smith, and Sukumar Kamalasadan are with the Department of Electrical and Computer Engineering, University of North Carolina at Charlotte, Charlotte, NC 28223 USA and also with the Energy Production Infrastructure Center, Department of Electrical Engineering, and Department of Engineering Technology and Construction Management, University of North Carolina at Charlotte, Charlotte, NC 28223 USA (e-mail: anair8@uncc.edu,; Michael.Smith@uncc.edu; skamalas@uncc.edu,).

Rojan Bhattarai is with the Department of Electrical and Computer Engineering, University of North Carolina at Charlotte, Charlotte, NC 28223 USA and also with the Idaho National Laboratories, Idaho Falls,, ID 83415 USA (e-mail: rbhattar@uncc.edu,).

Color versions of one or more of the figures in this article are available online at https://ieeexplore.ieee.org.

Digital Object Identifier 10.1109/TIA.2020.3035339

failure can inhibit the control approach from satisfying the performance requirements.

To address the issues associated with the dependency of the VC-based approach on measured values and sensors, an identification based control approach is proposed. This approach will reduce the significant effort required for tuning conventional static controllers with varying grid operating conditions. Moreover, the online identification of a system transfer function does not demand any foresight of system parameters. The major goal of this proposed work is to offer an improved DFIG control architecture that provides reduced dependency on sensors and increased operational stability over a wider operating region, without the need for further controller tuning. In earlier work [16], an identification based control approach to enhance the performance of the grid-side converter (GSC) was presented. This work is an expanded version of [16], which presents a novel identification based sensorless control approach for both rotor-side converter (RSC) and GSC control of a DFIG. The architecture is robust to any parameter variations due to the proposed additional voltage control loop. The other issue linked with DFIG operation variations is associated with irregularities in position and speed from the sensor(s) for the machine contributed due to sensor noise and malfunctioned speed or position sensors. Hence, researchers have attempted to propose sensorless speed control of DFIGs [17]. In this work, rotor speed and position are estimated from stator flux, calculated based on rotor measured quantities. This creates a dependency on rotor current sensors, which can negatively impact the robustness of the sensorless speed operation, as well as the operation of the conventional VC approach. Hence, in this work, the conventional VC is augmented with an adaptive control to ensure robustness and reduce the dependency on sensors. Significant attributes of the proposed technique include the following.

1) An online identification based adaptive control strategy that does not necessitate prior knowledge of system parameters.
2) The proposed robust architecture can be easily integrated with the existing conventional controller topology, without considerable structural changes.
3) The proposed control topology exhibits superior performance during dynamic grid operating conditions (e.g., load changes, faults, etc.).
4) The proposed control strategy is expandable to be implemented in real systems connected with larger power networks.
5) The proposed controller reduces the dependency of DFIG control on sensors, thereby making it more robust.

Compared to the earlier work [16], the proposed approach is new in the following aspects.

1) A new identification based control approach for the RSC of a DFIG coupled with an identification based controller on the GSC.
2) Additional voltage control loop added on the RSC controller contributing to the parametric robustness of the proposed controller.
3) Increased robustness by reducing susceptibility to measurement errors from current sensor faults in addition to the speed sensor proposed in earlier work [16].

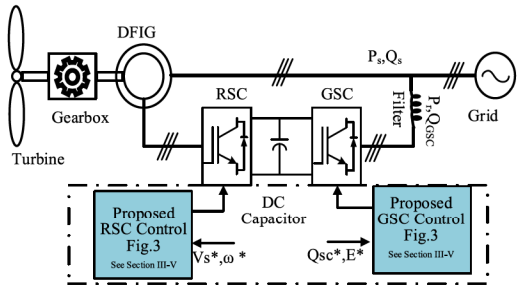

Fig. 1. General schematic of a DFIG.

4) Enhanced reactive power capability when operating under the unity power factor (UPF) mode, as well as the non-UPF mode of operation of the GSC.
5) Modification of the overall control architecture by appending identification based controller ensures superior performance under variable operating conditions, where the conventional static PI controller fails.

In this work, an estimation based adaptive speed control approach that augments the existing VC is presented. The results show that the proposed technique, augmented with the existing control logic, elevates the performance index of a DFIG-based system in case of any current or speed sensor failures. Subsequent sections organize the presented work, as follows. Section II discusses the details and mathematical equations governing the modeling for DFIG-based WECS. Section III describes the estimation technique for rotor speed that enables the sensorless operation of the DFIG, where Section III-C details the adaptive control design based on the identified parameters. The results are discussed in Section IV, with the conclusions following in Section V.

II. Modeling of DFIG

A general illustration of a DFIG-based wind turbine system with the proposed modification is shown in Fig. 1. The mathematical equations governing the operation of a DFIG in a synchronously rotating reference frame is presented here, which is similar to the arbitrary reference representation in [18]. The convention followed for modeling this work considers the outgoing current from the stator and the incoming current to the rotor-side as positive. The electrical equations of a DFIG based on a $\mathrm{d}-\mathrm{q}$ reference frame (rotating at synchronous speed) are given by

$$\begin{aligned} \mathrm{v}_{\mathrm{dqs}} &= -\mathrm{r}_{\mathrm{s}}\mathrm{i}_{\mathrm{dqs}} + \mathrm{j}\frac{\omega_{\mathrm{e}}}{\omega_{\mathrm{b}}}\Psi_{\mathrm{dqs}} + \mathrm{p}\frac{\Psi_{\mathrm{dqs}}}{\omega_{\mathrm{b}}} \\ \mathrm{v}'_{\mathrm{dqr}} &= -\mathrm{r}'_{\mathrm{r}}\mathrm{i}'_{\mathrm{dqr}} + \mathrm{j}\frac{\omega_{\mathrm{e}}-\omega_{\mathrm{r}}}{\omega_{\mathrm{b}}}\Psi'_{\mathrm{dqr}} + \mathrm{p}\frac{\Psi'_{\mathrm{dqr}}}{\omega_{\mathrm{b}}} \end{aligned} \tag{1}$$

$$\begin{aligned} \Psi_{\mathrm{dqs}} &= -\mathrm{L}_{\mathrm{ls}}\mathrm{i}_{\mathrm{dqs}} + \mathrm{L}_{\mathrm{m}}(\mathrm{i}_{\mathrm{dqs}} + \mathrm{i}'_{\mathrm{dqr}}) \\ \Psi'_{\mathrm{dqr}} &= -\mathrm{L}'_{\mathrm{lr}}\mathrm{i}'_{\mathrm{dqr}} + \mathrm{L}_{\mathrm{m}}(\mathrm{i}_{\mathrm{dqs}} + \mathrm{i}'_{\mathrm{dqr}}). \end{aligned} \tag{2}$$

The instantaneous value of real and reactive power output from the stator are given by

$$\begin{aligned} \mathrm{P}_{\mathrm{stator}} &= \mathrm{v}_{\mathrm{qs}}\mathrm{i}_{\mathrm{qs}} + \mathrm{v}_{\mathrm{ds}}\mathrm{i}_{\mathrm{ds}} \\ \mathrm{Q}_{\mathrm{stator}} &= \mathrm{v}_{\mathrm{qs}}\mathrm{i}_{\mathrm{ds}} + \mathrm{v}_{\mathrm{ds}}\mathrm{i}_{\mathrm{qs}} \end{aligned} \tag{3}$$

where (P_{stator}) is active power and (Q_{stator}) is reactive power output from the stator.

The proposal made in this work is based on some assumptions, as described below

1) Synchronously rotating stator flux oriented reference (i.e., $\Psi_{ds} = \Psi_s$, $\Psi_{qs} = 0$, and $v_{qs} = V_s$, $v_{ds} = 0$).
2) Negligible stator flux dynamics due to stronger grid (i.e., $p\Psi_{qs} = p\Psi_{ds} \approx 0$).

A. Model of RSC Control

RSC control depicted in Fig. 1, based on dq transformation, allows independent control of P_{stator} and Q_{stator} output from the stator.

The electrical relationships that govern the design of RSC control is given by

$$\begin{aligned} v'_{dr} &= r'_r i'_{dr} + p\frac{\sigma L'_r i'_{dr}}{\omega_b} - \omega_{slip}\left(\frac{\sigma L_s L'_r}{L_m} i_{qs} - \frac{r_s L'_r}{L_m} i_{ds}\right) \\ v'_{qr} &= r'_r i'_{qr} + p\frac{\sigma L'_r i'_{qr}}{\omega_b} - \cdots \\ &\quad \cdots \omega_{slip}\left(\frac{\sigma L_s L'_r}{L_m} i_{ds} - \frac{L'_r}{L_m}\left(v_{qs} + r_s i_{qs}\right)\right) \end{aligned} \tag{4}$$

where $\sigma = \dfrac{L'_r L_s - L_m^2}{L_s L'_r}$. Equation (4) describes the rotor voltages in the $d-q$ axis referred to the stator-side,

$$v'_{dr} = v''_{dr} + v'''_{dr} \tag{5}$$

$$v'_{qr} = v''_{qr} + v'''_{qr} \tag{6}$$

and

$$\begin{aligned} v''_{dr} &= \left(r'_r + p\frac{\sigma L'_r}{\omega_b}\right) i'_{dr} \\ v'''_{dr} &= -\omega_{slip}\left(\frac{\sigma L_s L'_r}{L_m} i_{qs} - \frac{r_s L'_r}{L_m} i_{ds}\right) \\ v''_{qr} &= \left(r'_r + p\frac{\sigma L'_r}{\omega_b}\right) i'_{qr} \\ v'''_{qr} &= -\omega_{slip}\left(\frac{\sigma L_s L'_r}{L_m} i_{ds} + \frac{L'_r}{L_m}\left(v_{qs} + r_s i_{qs}\right)\right). \end{aligned} \tag{7}$$

In (5) and (6)

1) The first component is in proportion to the d and q axis rotor current dynamics, respectively.
2) The second component represents the speed voltage that couples the $d-q$ axis components with one another.

Using the stated assumptions, (3) can be written as

$$\begin{aligned} P_s &= \frac{L_m v_{qs}}{L_s}\left(\frac{v''_{qr}}{r_r + p\dfrac{\sigma L_r}{\omega_b}}\right) \\ Q_s &= -\frac{v_{qs}\Psi_{ds}}{L_s} + \frac{L_m v_{qs}}{L_s}\left(\frac{v''_{dr}}{r_r + p\dfrac{\sigma L_r}{\omega_b}}\right). \end{aligned} \tag{8}$$

Equation (8) shows that by properly defining the v''_{qr} and v''_{dr} components of rotor voltages, the control logic for the P_{stator} and Q_{stator} output of a DFIG can be defined.

B. Model of GSC Control

The GSC modification presented in Fig. 1 focuses on maintaining a constant dc-link voltage. The GSC under a UPF mode of operation does not provide any additional reactive power support. However, in a non-UPF mode, the GSC control can regulate the reactive power flow between the converter and the stator/grid. Usually, the GSC control logic is designed based on a grid-voltage oriented reference frame. GSC control can regulate dc-link voltage with the d-axis current and reactive power for the q-axis.

$$\begin{bmatrix} V_{ai} \\ V_{bi} \\ V_{ci} \end{bmatrix} = R\begin{bmatrix} I_a \\ I_b \\ I_c \end{bmatrix} + pL\begin{bmatrix} I_a \\ I_b \\ I_c \end{bmatrix} + \begin{bmatrix} V_a \\ V_b \\ V_c \end{bmatrix} \tag{9}$$

In (9), R represents the line resistance and L is the line inductance. Using the parks transformation to convert an abc reference frame to a $d-q$ frame rotating at the angular frequency of the supply voltage, ω_e (in units of rad/s), (9) can be represented as

$$\begin{aligned} v_{di} &= Ri_d + pLi_d - \omega_e Li_q + v_d \\ v_{qi} &= Ri_q + pLi_q - \omega_e Li_d + v_q \end{aligned} \tag{10}$$

where i_d and i_q are the $d-q$ axis currents from the inverter, v_d and v_q are the $d-q$ axis grid voltages, and v_{di} and v_{qi} are the $d-q$ axis output voltages of the inverter. Thus, the controller aims at generating the proper voltage sequence to maintain the dc-link voltage and reactive power output.

III. Proposed Sensorless Adaptive Control Architecture

This work proposes sensorless control of a DFIG by estimating the rotor position and speed based on some measurable quantities. This is structured by designing an adaptive model based on an actual model formulated using measured rotor current [19], [20]. The rotor current is estimated by the adaptive model and adjusted continuously until it matches the reference model. Once the adaptive model exactly matches the reference model, the estimated parameters represent the actual system. The overall architecture is shown in Fig. 2.

A. Speed Observer and RLS Identifier for DFIG

For the adaptive model, the value of the rotor current $\hat{i}_r$ is estimated based on the stator voltage and current, v_s and i_s, respectively. The stator flux, in a stationary frame with i_r as the rotor current and θ_r as the rotor position with respect to the stationary reference frame, is represented as

$$\Psi_s = -L_s i_s + L_m i_r e^{j\theta_r}. \tag{11}$$

The estimated rotor current $\hat{i}_r$, with $\hat{\theta}_r$ representing the rotor angle estimation, is obtained as

$$\hat{i}_r = \frac{\psi_s + L_s i_s}{L_m} e^{-j\hat{\theta}_r}. \tag{12}$$

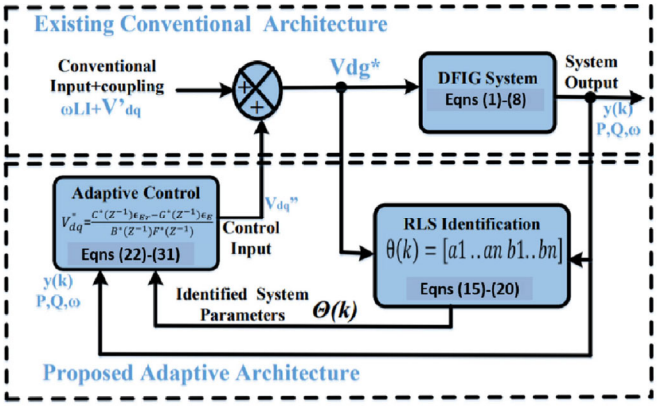

Fig. 2. General schematic of adaptive control with RLS.

Based on the magnitude and angle difference between measured and estimated value of the rotor current, an error function is formulated with currents expressed in $\alpha - \beta$ components. In this frame, the error function (calculated using atan2) can be written as

$$\epsilon = \text{atan2}\left(\frac{\mathrm{i_r} * \hat{\mathrm{i}}_\mathrm{r}}{\mathrm{i_r} \cdot \hat{\mathrm{i}}_\mathrm{r}}\right). \tag{13}$$

This approach has advantages over the conventional cross product based approach, since this approach ensures that the error is zero only when the measured and actual current vectors coincide with each other. An ideal small signal model of the proposed estimator is shown in (14), without considering any discontinuous effects, like delays and changes in the machine's physical parameters (resulting from conditions, such as temperature variations and misshaped voltage and current wave forms), which are discussed in [21]. A small signal error function model (where $\Delta\epsilon$ representing the error between the actual and measured rotor angle, $\Delta\omega_\mathrm{r}$ and $\Delta\hat{\omega_\mathrm{r}}$ are the deviations in the actual and estimated speed) can be represented as

$$\Delta\epsilon = \Delta\theta_{\mathrm{err}} = \frac{\Delta\omega_\mathrm{r} - \Delta\hat{\omega_\mathrm{r}}}{\mathrm{s}}. \tag{14}$$

Nonlinearities exhibited between the estimated rotor speed $\hat{\omega}_\mathrm{r}$ and the rotor angle error ϵ are identified using the recursive least square (RLS) technique. The identification can be represented in a general auto-regressive moving average form as [22], [23]

$$\epsilon_E(k) = \frac{B(z^{-1})}{A(z^{-1})} \times \mathrm{V''_{dq}(k)} + \frac{\mathrm{C}(z^{-1})}{\mathrm{A}(z^{-1})} \times \varrho(\mathrm{k}) \tag{15}$$

where

$$\begin{aligned} \mathrm{A}(z^{-1})\epsilon_E(k) &= \mathrm{B}(z^{-1})\mathrm{V''_{dq}(k)} + \mathrm{C}(z^{-1})\varrho(\mathrm{k}) \\ \mathrm{A}(z^{-1}) &= 1 + \mathrm{a_1}z^{-1} + \mathrm{a_2}z^{-2} + \cdots + \mathrm{a_n}z^{-\mathrm{n}} \\ \mathrm{B}(z^{-1}) &= \mathrm{b_1}z^{-1} + \mathrm{b_1}z^{-2} + \cdots + \mathrm{b_n}z^{-\mathrm{n}} \\ \mathrm{C}(z^{-1}) &= 1 + \mathrm{c_1}z^{-1} + \mathrm{c_2}z^{-2} + \cdots + \mathrm{c_n}z^{-\mathrm{n}} \end{aligned} \tag{16}$$

and, $k = n+1, n+2, \ldots, t$, t is the time index, $\mathrm{V''_{dq}(k)}$ is the RSC control input voltage sequence to the system, $\epsilon_E(k)$ is the output error sequence in rotor speed for active power control loop (d loop) or error in stator reactive power from reference for reactive power control loop (q loop) to be identified, and $\varrho(\mathrm{k})$ represents any form of disturbance or error. For a sensorless control loop, the error function defined by (13) is fed as the output of the system. A control input, which is the estimated rotor speed sequence, is then derived using a similar approach. The system coefficients to be identified, given by $\hat{\theta}(\mathrm{k})$, are predicted using (17). This is done by minimizing the error variance between the model output and the actual output, which is treated with a gain K [22], [24], such that

$$\hat{\theta}(\mathrm{k}) = \hat{\theta}(\mathrm{k}-1) + \mathrm{K(k)}[\epsilon_\mathrm{E}(\mathrm{k}) - \hat{\epsilon_\mathrm{E}}(\mathrm{k})] \tag{17}$$

where gain K and P are iteratively calculated as

$$K(k) = \frac{P(k-1)\phi(k+1)}{\lambda + \phi^T(k-1)P(k-1)\phi(k-1)} \tag{18}$$

$$P(k) = \frac{1}{\lambda}[I - K(k)\phi^T(k-1)]P(k-1) \tag{19}$$

and

$$\theta = \begin{bmatrix} a_1 & a_2 & b_1 & b_2 \end{bmatrix}. \tag{20}$$

B. Modification of Outer Voltage Control Loop

The ability to provide independent control of active and reactive power flow is one of the major advantages of the conventional VC approach. In a UPF mode of operation, the reactive power output is regulated by the RSC control. However, several parameters (e.g., varying operating conditions, grid parameter variations, and accumulation of speed estimation errors) can affect the control of reactive power flow. Hence, in this work the proposed additional outer voltage control loop, augmented with the RSC loop, derives the reference value of reactive power for the RSC converter control. The proposed outer loop is formulated considering the fraction of the total rotor current contributing toward the generation of reactive power. This portion of rotor current i^*_{drg}, as shown in Fig. 3, is derived considering the stator terminal voltage and mutual inductance [21]. This is based on the general equivalent circuit of a DFIG-based system. As the machine mutual inductance changes, the reactance of the branch between the stator and rotor-side reactance varies and this changes the amount of rotor current flowing through it. This varies the fraction of the rotor current contributing toward reactive power. The additional voltage control loop added in Fig. 3 will identify the reactive power reference for maintaining the stator terminal voltage, considering the effect of parameter variations. The stator terminal voltage is maintained at 1 p.u ($Vs^* = 1$ p.u). The reactive power derived from the stator has a magnetizing component, as well as a reactive power generating component. If it is assumed at a no load condition that all the magnetizing reactive power is supplied from the rotor, the stator reactive power will only be responsible for reactive power generation [25]. Under such conditions, with stator transients neglected, (1) can be modified to estimate mutual inductance, as shown in (21).

$$L_m = \frac{v_{\mathrm{qs}} + r_s i_{\mathrm{qs}}}{i_{\mathrm{drm}}} \tag{21}$$

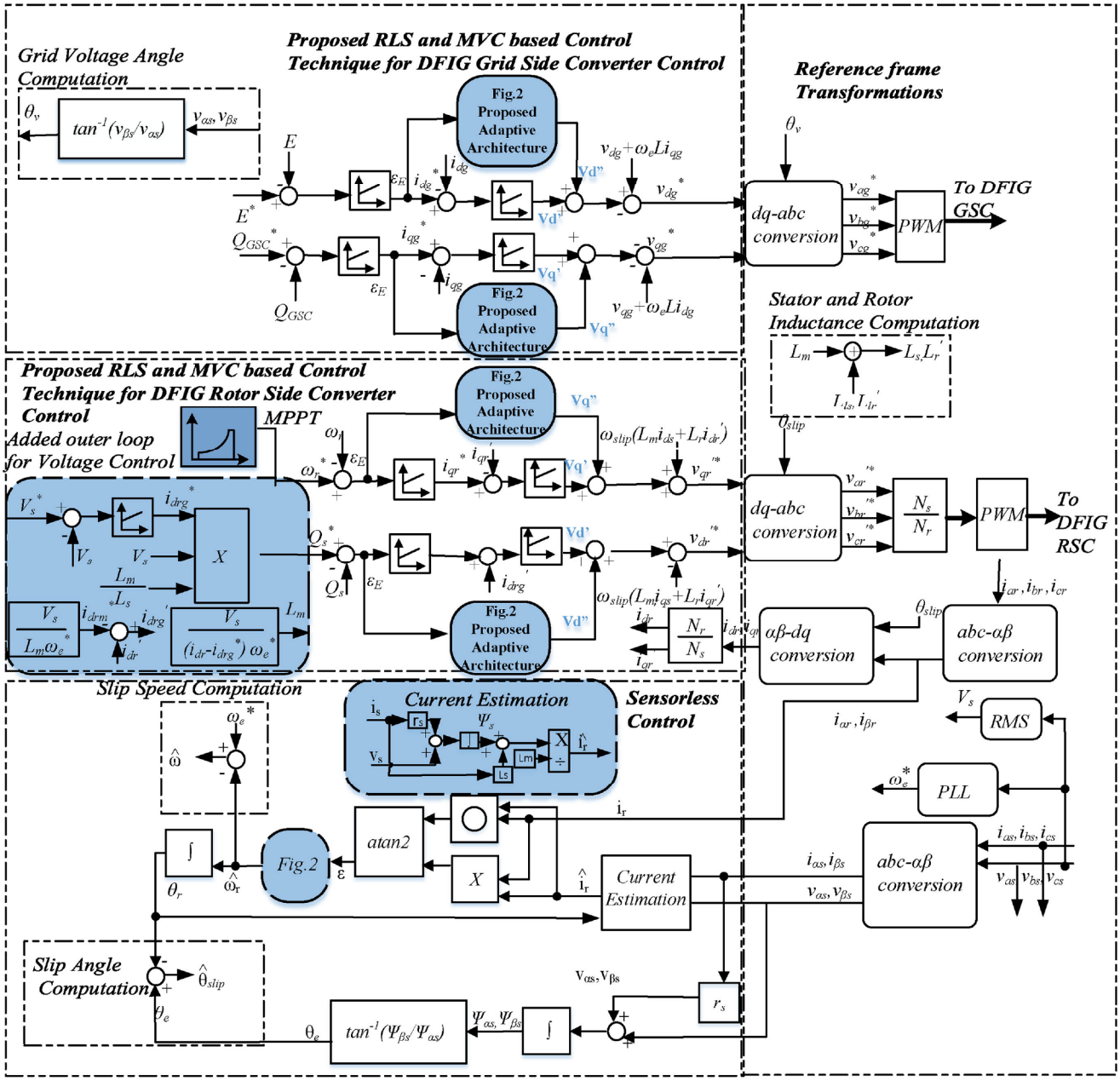

Fig. 3. Proposed identification based modified control architecture of DFIG.

The i_{drm} for L_m identification is obtained as $i_{dr} - i_{\mathrm{drg}}$, where $i_{\mathrm{drg}} = i^*_{\mathrm{drg}}$ is derived from the outer voltage loop for the reactive power reference. The proposed loop is expected to provide superior reactive power control on a sensorless system during variable grid conditions.

C. Minimum Variance Control

Minimum variance control (MVC) is a self-tuning based control algorithm that aims at minimizing the variance of the controlled outputs. This control method is superior to conventional control for its ability to minimize the deviations of the controlled signal, ability to be implemented in any system without required prior knowledge of system parameters, and ability to follow and derive a control sequence based on parameter variations. This control has the ability to consider the dynamic disturbances occurring during practical situations, without any prior system knowledge [22], [24], [26].

For the MVC design process, consider the system described in (15), where $\mathrm{u(k)}$ is the control signal (which is the rotor RSC voltage sequence), $\mathrm{y(k)}$ is the output of the overall system (which is the error between actual and reference value), $\varrho(k)$ is a sequence of independent normal variables with zero mean value and variance of one (white noise). Consider the system model in (15), which can be written as

$$\epsilon_{\mathrm{E}}(\mathrm{k}) = \frac{\mathrm{B}^*(\mathrm{z}^{-1})}{\mathrm{A}^*(\mathrm{z}^{-1})}\mathrm{z}^{-\mathrm{d}}\mathrm{V}''_{\mathrm{dq}}(\mathrm{k}) + \frac{\mathrm{C}^*(\mathrm{z}^{-1})}{\mathrm{A}^*(\mathrm{z}^{-1})}\varrho(\mathrm{k}) \qquad (22)$$

where d is any excess pole, if present in the system. Matrices A, B, and C are identified by the RLS algorithm. System output $\epsilon_{\mathrm{E}}(\mathrm{k}+\mathrm{d})$ predicted "d" steps into the future yields,

$$\epsilon_{\mathrm{E}}(\mathrm{k}+\mathrm{d}) = \frac{\mathrm{C}^*(\mathrm{z}^{-1})}{\mathrm{A}^*(\mathrm{z}^{-1})}\varrho(\mathrm{k}+\mathrm{d}) + \frac{\mathrm{B}^*(\mathrm{z}^{-1})}{\mathrm{A}^*(\mathrm{z}^{-1})}\mathrm{V}''_{\mathrm{dq}}(\mathrm{k})$$

$$= \mathrm{F}^*(\mathrm{z}^{-1})\varrho(\mathrm{k}+\mathrm{d}) + \frac{\mathrm{G}^*(\mathrm{z}^{-1})}{\mathrm{A}^*(\mathrm{z}^{-1})}\varrho(\mathrm{k}) + \frac{\mathrm{B}^*(\mathrm{z}^{-1})}{\mathrm{A}^*(\mathrm{z}^{-1})}\mathrm{V}''_{\mathrm{dq}}(\mathrm{k}) \quad (23)$$

where (24) relates $\mathrm{F}^*(\mathrm{z}^{-1})$ and $\mathrm{G}^*(\mathrm{z}^{-1})$ with $\mathrm{C}^*(\mathrm{z}^{-1})$

$$\mathrm{C}^*(\mathrm{z}^{-1}) = \mathrm{A}(\mathrm{z}^{-1})\mathrm{F}(\mathrm{z}^{-1}) + \mathrm{z}^{-\mathrm{d}}\mathrm{G}(\mathrm{z}^{-1}). \quad (24)$$

Estimating error $\varrho(k)$ from the original model gives

$$\varrho(\mathrm{k}) = \frac{\mathrm{A}^*(\mathrm{z}^{-1})\epsilon_{\mathrm{E}}(\mathrm{k}) - \mathrm{B}^*(\mathrm{z}^{-1})\mathrm{z}^{-\mathrm{d}}\mathrm{V}''_{\mathrm{dq}}(\mathrm{k})}{\mathrm{C}^*(\mathrm{q}^{-1})}. \quad (25)$$

Substituting $\varrho(\mathrm{k})$ in (23) gives

$$\epsilon_{\mathrm{E}}(\mathrm{k}+\mathrm{d}) = \mathrm{F}^*\varrho(\mathrm{k}+\mathrm{d}) + \frac{\mathrm{G}^*}{\mathrm{C}^*}\epsilon_{\mathrm{E}}(\mathrm{k}) + \frac{\mathrm{B}^*\mathrm{F}^*}{\mathrm{C}^*}\mathrm{V}''_{\mathrm{dq}}(\mathrm{k}). \quad (26)$$

The adaptive control logic calculates the ideal input sequence $\mathrm{u}(\mathrm{k})$, such that the error between the reference input and the predicted output is minimized using the function given below

$$\mathrm{J} = \mathrm{E}\{[\epsilon_{\mathrm{E}}(\mathrm{k}+\mathrm{d}) - \epsilon_{\mathrm{Er}}]^2\}. \quad (27)$$

In (27), E represents the expectation of difference between the estimated output and the reference input to the system $\epsilon_{\mathrm{E}r}$. Using (26) and (27), the cost function is minimized when

$$\mathrm{E}\left\{\left(\frac{\mathrm{G}^*}{\mathrm{C}^*}\epsilon_{\mathrm{E}}(\mathrm{k}) - \epsilon_{\mathrm{Er}} + \frac{\mathrm{B}^*\mathrm{F}^*}{\mathrm{C}^*}\mathrm{V}''_{\mathrm{dq}}(\mathrm{k})\right)^2\right\}$$

is zero. The white noise $\varrho(\mathrm{k})$ does not correlate with other terms in the abovementioned equation. Thus, the optimal control sequence is obtained as (28).

$$\mathrm{V}''_{\mathrm{dq}}(\mathrm{k}) = \frac{C^*(z^{-1})\epsilon_{\mathrm{E}r} - G^*(z^{-1})\epsilon_{\mathrm{E}}(\mathrm{k})}{B^*(z^{-1})F^*(z^{-1})} \quad (28)$$

The control sequence applied to the system model in (15) yields

$$\mathrm{A}^*(\mathrm{z}^{-1})\epsilon_{\mathrm{E}}(\mathrm{k}) = -\frac{\mathrm{G}^*(\mathrm{z}^{-1})}{\mathrm{F}^*(\mathrm{z}^{-1})}\mathrm{z}^{-\mathrm{d}}\epsilon_{\mathrm{E}}(\mathrm{k}) + \frac{\mathrm{C}^*(\mathrm{z}^{-1})}{\mathrm{F}^*(\mathrm{z}^{-1})}\epsilon_{\mathrm{Er}} + \mathrm{C}^*(\mathrm{z}^{-1})\varrho(\mathrm{k}). \quad (29)$$

After algebraic manipulation with the use of (24), the following expression is produced

$$\frac{\mathrm{C}^*(\mathrm{z}^{-1})}{\mathrm{F}^*(\mathrm{z}^{-1})}\epsilon_{\mathrm{E}}(\mathrm{k}) = \frac{\mathrm{C}^*(\mathrm{z}^{-1})}{\mathrm{F}^*(\mathrm{z}^{-1})}\epsilon_{\mathrm{Er}} + \mathrm{C}^*(\mathrm{z}^{-1})\varrho(\mathrm{k}). \quad (30)$$

Thus,

$$\epsilon_{\mathrm{E}}(\mathrm{k}) = \epsilon_{\mathrm{Er}} + \mathrm{F}^*(\mathrm{z}^{-1})\varrho(\mathrm{k}). \quad (31)$$

The control input sequence for both the RSC and the GSC dq loop and rotor speed estimation are derived in this similar manner. System identification based MVC control is shown in Fig. 2. The overall proposed control architecture with identification is shown in Fig. 3. The RSC and GSC modifications, along with the identification based sensorless approach and the additional voltage control loop (with parameter robustness), are detailed in the overall architecture provided in Fig. 3.

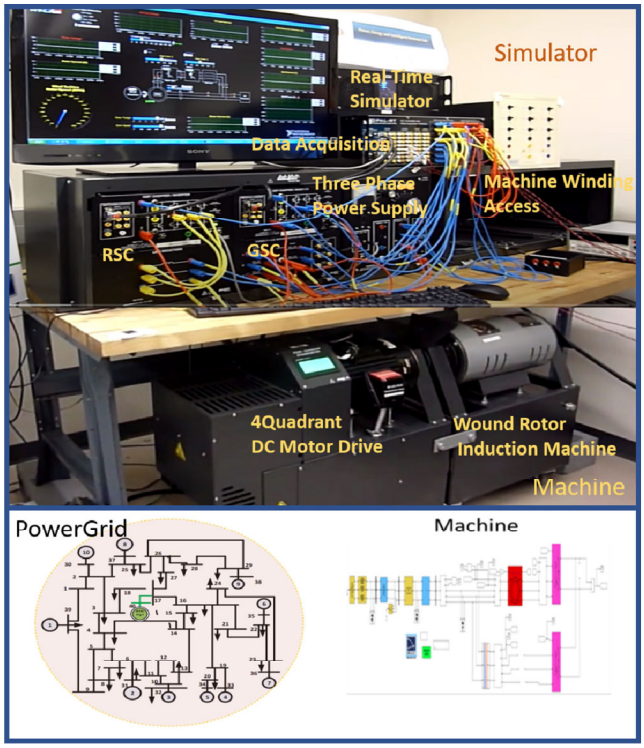

Fig. 4. Schematic of HIL real-time simulations performed with OPAL-RT.

IV. Results and Discussion

For the experimental results, we use a GE 1.5 MW wind turbine model in the real-time simulator (OPAL-RT platform) and a 2 KW WTG (4 quadrant dc motor drive and a wound rotor induction machine- Lab-Volt 8013-A, [27]) for the hardware-in-the-loop (HIL) test set up that characterizes the GE 1.5 MW model. The specifications are included in Tables VII and VIII, respectively. The models and the hardware WTG is integrated with the simulator. The RSC and GSC are also integrated into the controller that is designed using the real-time simulator. For sensing, a data acquisition kit (OP 8660) is used. A three-phase power supply integrated with the simulator is used to connect with the grid as a rigid infinite source for the first set of experiments. For the second set of experiments, the rigid source is controlled by an external signal derived from the real-time grid model (IEEE 39 bus system) designed in the real-time simulator. The details are shown in Fig. 4. This is a fully integrated HIL testbed (for both power and control).

A. Test 1: Performance Analysis for Sensorless Operation

The first test set is used to evaluate the efficiency of the proposed architecture for its sensorless operation and its robustness to sensor failures with a hard grid (single machine infinite bus mode).

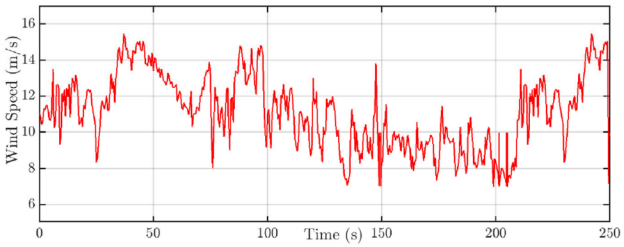

Fig. 5. Case 1: Dynamic wind speed data to test the performance of proposed controller.

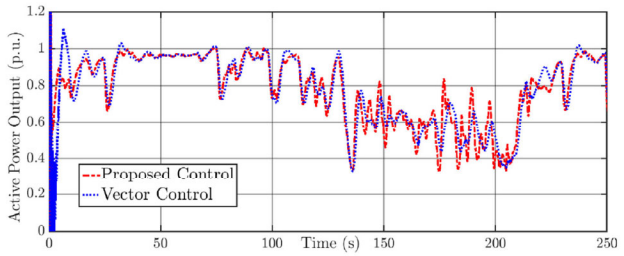

Fig. 6. Test 1: Active power output from DFIG for variable wind speed shown in Fig. 5.

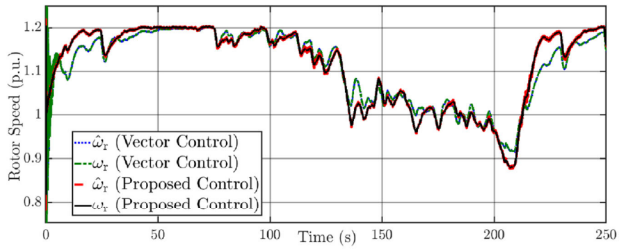

Fig. 7. Case 1: Estimated rotor speed for a DFIG with the proposed control technique and conventional technique.

1) Case 1: Validation of Proposed Architecture With Real Dynamic Wind Data: To validate the performance of the proposed approach in the real world, the performance is tested with dynamic-wind data obtained from [28] which is shown in Fig. 5. The modification to the GSC and RSC loop with sensorless architecture is compared with the conventional control approach on the GSC and RSC with the proposed speed estimation technique. Fig. 6 illustrates the power profile. Fig. 6 shows a comparison between the total power generated from the DFIG using VC and the proposed identification based control for wind speed (shown in Fig. 5) operating under maximum power point tracking (MPPT) mode, as shown in Fig. 3. Performance variations can be attributed to the difference in controller parameters and response time. The faster response characteristics of the proposed controller can be seen in Fig. 6. Fig. 7 shows the comparison of rotor speed estimation between VC and the proposed architecture. The proposed sensorless estimation technique was successful for the DFIG control approach. The estimated rotor speed can be found closely following the actual rotor speed with an estimation error of 2.2% compared to 4.95% for conventional control, as shown in Table I. The torsional stress comparisons between VC and the proposed controller is shown in Table II.

TABLE I
PERFORMANCE COMPARISON BASED ON TEST 1

Control Architecture	Percentage Absolute Error (%)		Percentage Mean Error (%)	
	VC	Proposed	VC	Proposed
V_{PCC}	1.52	0.71	0.0003	0.11
ω_r	4.95	2.2	0.07	0.0012
E	3.67	2.67	0.081	0.0067
Q_{GSC}	0.22	0.42	0.0006	0.0014

TABLE II
QUANTITATIVE COMPARISON OF ROTOR SHAFT TORSIONAL STRESS WITH THE PROPOSED ARCHITECTURE AND THE CONVENTIONAL ARCHITECTURE

Control	Pm-Pe Difference (p.u.)	Mean Absolute Difference (p.u.)
Proposed	0.7466	0.1101
VC	0.7873	0.1268

TABLE III
SENSOR STATUS USED FOR PERFORMING CASE 2

Duration (s)	Sensors
0-5	RSC and GSC Current & Speed Sensor
5+	GSC Current & Speed Sensor

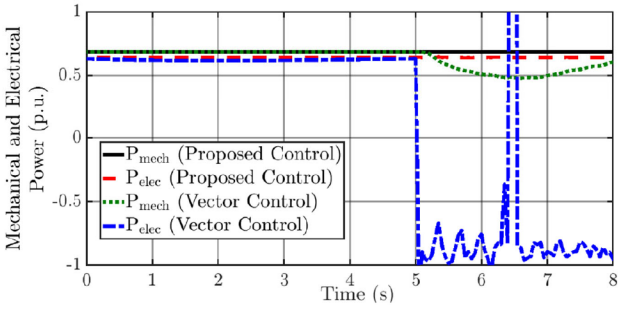

Fig. 8. Case 2: Comparison of power balance between mechanical and electrical side of DFIG during rotor current sensor failure.

2) Case 2: Rotor Current Sensor Dependency Analysis of Proposed Architecture: The main objective of this work is to enhance the controller performance by reducing its dependency on sensors. Since conventional control completely relies on the sensor-based rotor current measurement, any sensor issues can impact the performance of the DFIG-based system. To analyze the proposed system performance efficiency, the system was tested with a simulated rotor current sensor failure scenario. The rotor sensor is turned OFF after 5 s assuming no measurement data are available after 5 s due to a bad sensor, as shown in Table III. As the proposed control loop can dynamically adjust the variation in feedback current due to current sensor failure, it can still maintain a stable operation as shown in Fig. 8. Thus, the proposed approach can be more economical by avoiding uncontrolled wind turbine downtime events resulting from sensor failures. Fig. 9 shows the rotor speed of the DFIG following a rotor current sensor fault.

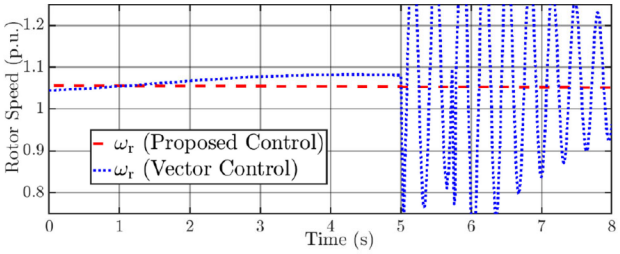

Fig. 9. Case 2: Comparison between DFIG rotor speed following a rotor current sensor failure with VC and proposed identification based control.

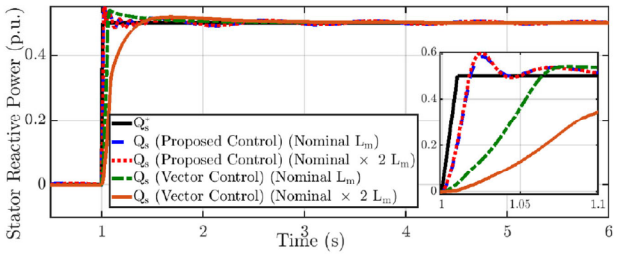

Fig. 10. Case 3: Stator reactive power tracking capability during machine mutual inductance variation.

TABLE IV
RESPONSE CHARACTERISTICS FOR CASE 3

Control Approach	Rise Time (s)	Settling Time (s)	Overshoot
Vector Control	0.4	0.7	5.5%
Proposed Control	0.07	3.7	1.8%

3) Case 3: Robustness of Proposed Architecture for Machine Parameter Variation: Variations in machine parameters (resulting from varying operating conditions) will be accounted for with the proposed architecture, since it is based on an online identification technique. Case 3 showcase this feature of the proposed approach by testing the system under a nominal machine mutual inductance value L_m and with double the nominal value. Fig. 10 illustrates the controller performance for a step-change in stator reactive power reference (Q_s^*) with machine parametric variation. It can be seen from Table IV and Fig. 10 that the proposed framework provides better reference tracking capability with faster settling even during parameter variations compared to conventional VC approach.

4) Case 4: Robustness of Proposed Architecture to Rotor Speed Sensor Failure: The capability of the proposed architecture to maintain operational reliability when subjected to a rotor speed sensor failure was analyzed in Case 4. A rotor speed sensor failure was created for a short duration of 0.2 s over a 5-s simulation. The proposed architecture, which relies on estimated speed based on rotor current, offers stable and reliable operation (even during the sensor failure), while the conventional control approach fails, as depicted in Fig. 11 and Table V.

B. Test 2: Scalability Test for The Proposed Controller

The second test evaluates the performance of proposed architecture in a scaled system. The performance of the proposed controller for the grid was validated using a scalability test performed on an IEEE 39 bus system, as shown in Fig. 12. In this

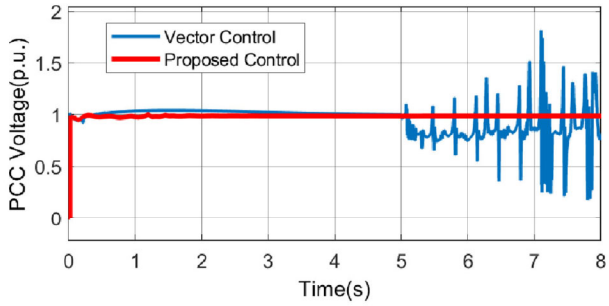

Fig. 11. Case 4: PCC voltage during speed sensor failure.

TABLE V
CASE 4: ROBUSTNESS ANALYSIS OF PROPOSED APPROACH TO PARAMETER VARIATION

Control Approach	Parameter	R.T (s)	S.T (s)	Overshoot (%)
Vector Control	N L_m	0.06	0.6	7.5
Vector Control	N × 2 L_m	0.25	1.05	3.5
Proposed Control	N L_m	0.02	0.4	12
Proposed Control	N × 2 L_m	0.02	0.4	13

Note: N implies nominal, R.T is rise time, S.T is settling time.

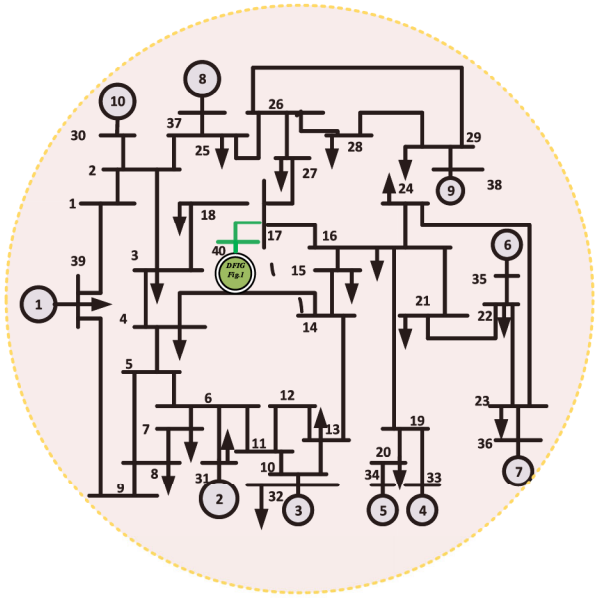

Fig. 12. Modified one-line diagram of IEEE 39 bus system with DFIG.

test, the proposed DFIG-based system was integrated to Bus 17 through a line impedance and virtual node Bus 40. The objective was to test the system performance for various grid dynamic conditions on the larger test system (e.g., fault, load change, and sudden reactive power demand). For a fault at the PCC, a terminal voltage as low as 0.2 p.u. was observed, 0.85 p.u for a load change, and 0.92 p.u for a sudden reactive power demand. These grid conditions were created in the simulation by varying the impedance on the Z_{line} interconnecting Bus 17 with virtual node Bus 40.

$$\mathrm{V_{Bus40}} = \mathrm{V_{Bus17}} \pm \mathrm{Z_{line}I} \tag{32}$$

As the line impedance increases, a weak grid scenario occurs, which can reduce or vary the PCC voltage corresponding to

TABLE VI
QUANTITATIVE ANALYSIS OF SCALABILITY TEST RESULTS

Test Scenario	Parameter Monitored	Vector Control	Proposed Control
Case1	V_{PCC} Steady State Error	0.8%	0.6%
Case2	Q_{PCC} Settling Time	0.16%	0.02%
Case3	V_{PCC} Dip	NA	13.53% < VC

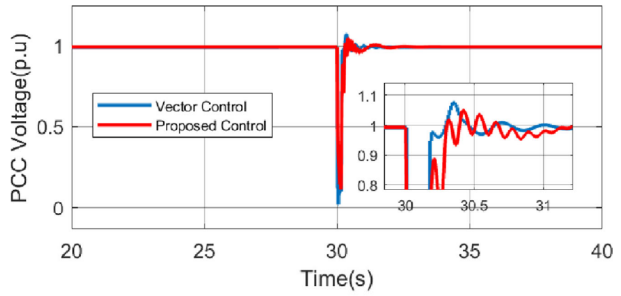

Fig. 13. Case 1: Comparison of PCC Voltage in response to voltage sag due to grid fault.

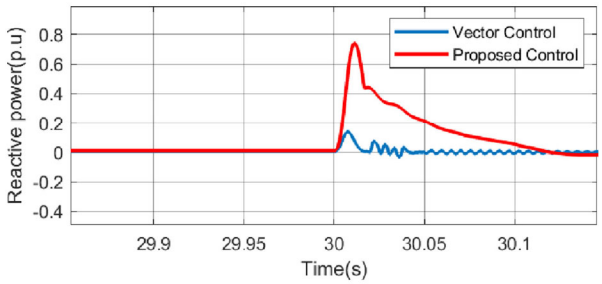

Fig. 14. Case 1: Comparison of reactive power output in response to voltage sag due to grid fault.

these different test scenarios. This test scenario was created by adjusting the line impedance, based on (32), to create the corresponding grid conditions. Unlike the conventional control architecture, the proposed adaptive architecture offers superior performance without any further retuning. Table VI shows the quantitative analysis of the scalability test that validates the superiority of the proposed control architecture over the conventional architecture.

1) Case 1: Performance Analysis for Three Phase to Ground Fault: The system was tested for a three-phase to ground fault at 30 s for a duration of 150 ms. Fig. 13 shows the PCC voltage for a weak grid scenario with a fault. The proposed control approach offered lower voltage overshoot, faster response, and less steady-state error. Fig. 14 shows the comparison of reactive power output in response to voltage sage to grid fault. Fig. 15 shows the corresponding $d-$ axis rotor current. The maximum value of rotor current is less than 0.25 p.u, which shows that the current carried by the converter during the event is less than 30% of the total machine rating. In general, a DFIG uses converters with a reduced rating (e.g., 30% of the total power rating). Hence, the current carried by the converter during the event is within the rating of the converter.

2) Case 2: Analysis of Reactive Power Support Capability: The performance of the system was tested for a sudden reactive

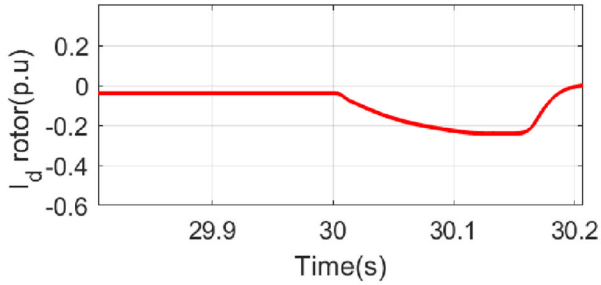

Fig. 15. Case 1: Rotor current corresponding to the reactive power support during fault.

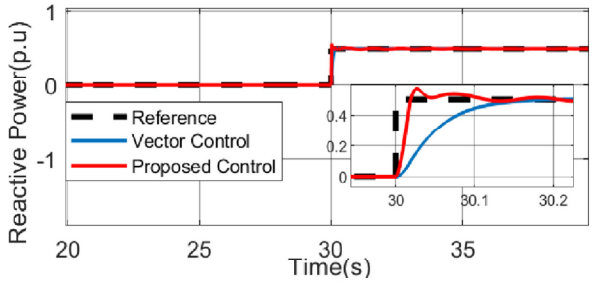

Fig. 16. Case 2: Comparison of reactive power tracking capability.

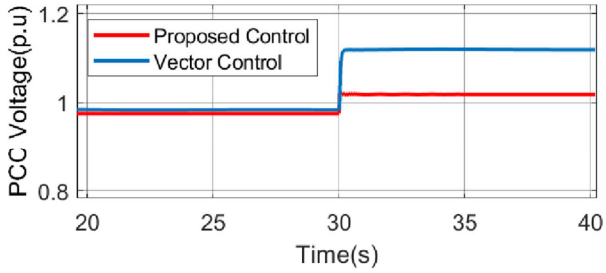

Fig. 17. Case 2: Comparison of PCC Voltage in response to reactive power demand.

power demand initiated at 10 s. Fig. 16 shows the improved reactive power support capability with the proposed system. With the proposed control loop, the system was able to more quickly provide additional reactive power demand, as shown in Table VI in terms of the reactive power control loop settling time. This is mainly attributed to the faster control action of the proposed identification based control over the conventional static control. The initial oscillatory nature in the proposed control can be attributed to the online identified transfer function capturing small dynamics in the system. The controller response is modified based on these effects. The settling time for reactive power at the point of common coupling (PCC) of the proposed system was as low as 0.02 s, in contrast to 0.16 s for the conventional control approach. Fig. 17 shows the superiority of the proposed system to maintain PCC voltage deviations, whereas maintaining the reactive power demand. For the proposed system, smaller voltage deviations were noticed to produce the same additional reactive power at 10 s.

3) Case 3: Performance Analysis for Sudden Load Variations: The performance of the system was tested for a sudden load variation occurring between 15 and 17 s. Fig. 18 shows

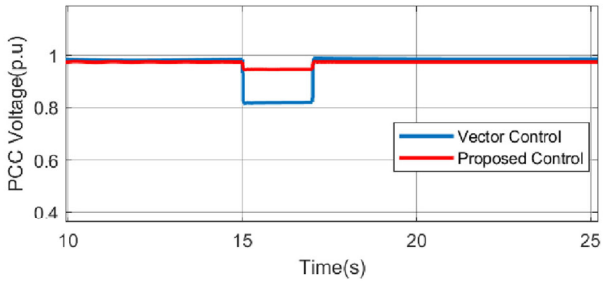

Fig. 18. Case 3: Comparison of PCC Voltage in response to load variations.

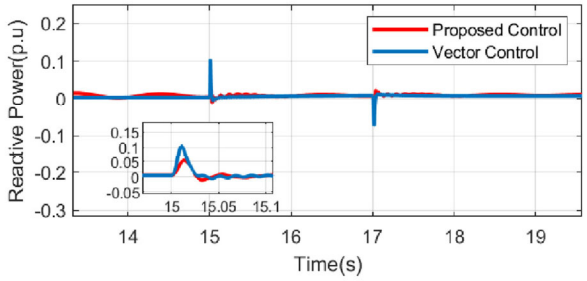

Fig. 19. Case 3: Reactive power support offered in response to load variations.

TABLE VII
DFIG AND CONVERTER PARAMETERS

Parameter	Value
Capacity, Rated	1.5 MVA
Voltage, Rated	575 V L-L
Stator resistance (r_s)	0.0071 p.u.
Stator ref. rotor resistance (r'_r)	0.005 p.u.
Stator leakage inductance (L_{ls})	0.1714 p.u.
Stator ref. rotor leakage inductance (L'_{lr})	0.1563 p.u.
Mutual inductance (L_m)	5.8 p.u.
Number of pole pairs (p)	3
Generator Inertia Constant (H_g)	0.5 s
Turbine Inertia Constant (H_t)	4.5 s
Simulation Time Step (T_s)	50 μs
Identification Time Step (T_i)	5 ms
MVC Time Step (T_c)	2 ms
DC Link Voltage	1100V
Capacitor	0.1 F
Grid coupling inductor	1mH
Grid frequency	60Hz
Grid Voltage	60Hz
Controller Parameters	
$K_{pd_{GSC}}$	1
$K_{id_{GSC}}$	0.5
$K_{pq_{GSC}}$	5
$K_{iq_{GSC}}$	10
$K_{pd_{RSC}}$	2
$K_{id_{RSC}}$	0.1
$K_{pq_{RSC}}$	0.5
$K_{iq_{RSC}}$	1

the ability of the proposed system to maintain the nominal terminal voltage during sudden load variations. The voltage dip resulting from sudden load variations was 13.53% smaller with the proposed control approach, compared to VC. Table VI shows the percentage dip in PCC voltage from the desired value for both

TABLE VIII
PARAMETERS OF WRIM USED IN HIL

Parameter	Value
Rated Capacity	2 KW
Rated Voltage	120/208 V
Rotor Winding Voltage	624 V L-L
Stator resistance (r_s)	0.6 Ω
Rotor resistance (r_r)	4.3 Ω
Power factor	0.72
Number of pole pairs (p)	2
Simulation Time Step (T_s)	50 μs
Rated frequency	60Hz

control architectures during load variations. The ability of the proposed approach to return the system to the desired nominal value during dynamic load conditions with minimum voltage variations and additional reactive power support is depicted in Fig. 19. Table VII illustrates the DFIG and converter parameters used in all the test cases. The simulations are carried out considering the turbine inertia (the value is specified in Table VII). The sampling frequency, converter, and controller parameters are all detailed in Table VII.

V. CONCLUSION

A system identification based modification of a conventional VC architecture is proposed in this article. As in the conventional approach, the proposed methodology offers decoupled control of active and reactive power of a DFIG, but independent of any sensor failures and parameter variation. The design approach details are presented and implementation of the proposed control methodology is explained with validation via several different test case scenarios, which depict the superiority of the proposed approach. The test results summarized in Table I through Table VI validate the claims of the proposed approach. The results show the improved operational reliability, robustness, and independent operation of a DFIG-based WECS with the proposed system identification based approach. The purposed work can be further enhanced by considering system identification based on multiple inputs for an improved (e.g., faster) response during dynamic conditions.

REFERENCES

[1] W. Leonhard, *Control of Electrical Drives*. Berlin, Germany: Springer, 2001.
[2] B. K. Bose and B. K. Bose, *Power Electronics and Variable Frequency Drives: Technology and Applications*, vol. 2. New York, NY, USA: Wiley, 1997.
[3] R. Cardenas, R. Pena, S. Alepuz, and G. Asher, "Overview of control systems for the operation of DFIGs in wind energy applications," *IEEE Trans. Ind. Electron.*, vol. 60, no. 7, pp. 2776–2798, Jul. 2013.
[4] M. Loucif and A. Boumédiène, "Modeling and direct power control for a DFIG under wind speed variation," in *Proc. 3rd Int. Conf. Control, Eng. Inf. Technol.*, May 2015, pp. 1–6.
[5] M. J. Zandzadeh, A. Vahedi, and A. Zohoori, "A novel direct power control strategy for integrated DFIG/active filter system," in *Proc. 20th Iranian Conf. Elect. Eng.*, May 2012, pp. 564–568.
[6] B. Lu, Y. Li, X. Wu, and Z. Yang, "A review of recent advances in wind turbine condition monitoring and fault diagnosis," in *Proc. IEEE Power Electron. Mach. Wind Appl.*, Jun. 2009, pp. 1–7.

[7] M. Reder, E. Gonzalez, and J. J. Melero, "Wind turbine failures-tackling current problems in failure data analysis," in *Proc. J. Phys., Conf. Ser.*, 2016, Art. no. 072027.
[8] S. Yang and V. Ajjarapu, "A speed-adaptive reduced-order observer for sensorless vector control of doubly fed induction generator-based variable-speed wind turbines," *IEEE Trans. Energy Convers.*, vol. 25, no. 3, pp. 891–900, Sep. 2010.
[9] K. Rothenhagen and F. W. Fuchs, "Doubly fed induction generator model-based sensor fault detection and control loop reconfiguration," *IEEE Trans. Ind. Electron.*, vol. 56, no. 10, pp. 4229–4238, Oct. 2009.
[10] Y. Majdoub, A. Abbou, and M. Akherraz, "Variable speed control of DFIG-wind turbine with wind estimation," in *Proc. Int. Renewable Sustain. Energy Conf.*, Oct. 2014, pp. 268–274.
[11] B. Bossoufi *et al.*, "Robust adaptive backstepping control approach of DFIG generators for wind turbines variable-speed," in *Proc. Int. Renewable Sustain. Energy Conf.*, Oct. 2014, pp. 791–797.
[12] M. Benbouzid, B. Beltran, H. Mangel, and A. Mamoune, "A high-order sliding mode observer for sensorless control of DFIG-based wind turbines," in *Proc. 38th Annu. Conf. IEEE Ind. Electron. Soc.*, Oct. 2012, pp. 4288–4292.
[13] A. B. Ataji, Y. Miura, T. Ise, and H. Tanaka, "Direct voltage control with slip angle estimation to extend the range of supported asymmetric loads for stand-alone DFIG," *IEEE Trans. Power Electron.*, vol. 31, no. 2, pp. 1015–1025, Feb. 2016.
[14] R. Maharjan and S. Kamalasadan, "Real-time simulation for active and reactive power control of doubly fed induction generator," in *Proc. North Amer. Power Symp.*, 2013, pp. 1–6.
[15] R. Maharjan and S. Kamalasadan, "A novel online adaptive sensorless identification and control of doubly fed induction generator," in *Proc. IEEE PES Gen. Meeting* Conf. Expo.|, 2014, pp. 1–5.
[16] A. R. Nair, R. Bhattarai, and S. Kamalasadan, "A sensorless adaptive grid side control approach for doubly fed induction generator (DFIG)," in *Proc. IEEE Industry Appl. Soc. Annu. Meeting*, Sep. 2019, pp. 1–10.
[17] G. Yuan, Y. Li, J. Chai, and X. Jiang, "A novel position sensor-less control scheme of doubly fed induction wind generator based on MRAS method," in *Proc. IEEE Power Electron. Specialists Conf.*, Jun. 2008, pp. 2723–2727.
[18] B. Wu, Y. Lang, N. Zargari, and S. Kouro, *Power Conversion and Control of Wind Energy Systems*. New York, NY, USA: Wiley, 2011.
[19] B. Touaiti, H. Ben Azza, and M. Jemli, "A MRAS observer for sensorless control of wind-driven doubly fed induction generator in remote areas," in *Proc. 17th Int. Conf. Sci. Techn. Autom. Control Comput. Eng.*, Dec. 2016, pp. 526–531.
[20] J. Yang *et al.*, "Sensorless control of brushless doubly fed induction machine using a control winding current MRAS observer," *IEEE Trans. Ind. Electron.*, vol. 66, no. 1, pp. 728–738, Jan. 2019.
[21] A. R. Nair, R. Bhattarai, and S. Kamalasadan, "Parametrically robust mutual inductance estimation based adaptive control architecture for doubly fed induction generator (DFIG)," in *Proc. IEEE Energy Convers. Congr. Expo.*, Sep. 2019, pp. 434–441.
[22] L. Ljung, *System Identification: Theory for the User*. London, U.K.: Pearson, 1998.
[23] M. Beza and M. Bongiorno, "A modified RLS algorithm for online estimation of low-frequency oscillations in power systems," *IEEE Trans. Power Syst.*, vol. 31, no. 3, pp. 1703–1714, May 2016.
[24] K. Åström and B. Wittenmark, *Adaptive Control: Second Ed.* (Series Dover Books on Electrical Engineering). New York, NY, USA: Dover, 2013. [Online]. Available: https://books.google.com/books?id=4CLCAgAAQBAJ
[25] R. Bhattarai, N. Gurung, S. Ghosh, and S. Kamalasadan, "Parametrically robust dynamic speed estimation based control for doubly fed induction generator," *IEEE Trans. Industry Appl.*, vol. 54, no. 6, pp. 6529–6542, Nov./Dec. 2018.
[26] J. Hetthéssy and L. Keviczky, "Minimum variance control a review and outlook," *Periodica Polytechnica Elect. Eng.*, vol. 21, no. 1, pp. 31–45, 1977.
[27] "Opal-rt 2kw HIL doubly-fed induction generator (DFIG) demo," Accessed: Oct. 2020. [Online]. Available: https://youtu.be/pFkJSz9lFDg
[28] "Wind speed profile," Accessed: Oct. 2020. [Online]. Available: http://www.ercot.com/mktinfo/rtm/

Anuprabha Ravindran Nair (Graduate Student Member, IEEE) received the B.Tech. degree in electrical engineering from Calicut University, Malappuram, India, in 2010, the M.S. degree in electrical engineering from Purdue University, West Lafayette, IN, USA, in 2016. She has been working toward the Ph.D. degree in electrical engineering from the Department of Electrical and Computer Engineering, University of North Carolina at Charlotte, Charlotte, NC, USA, since 2017. Her research interests include renewable energy integration and stability, DFIG-based WECS, modeling and analysis of weak grid, power system stability, and control, integration of distributed energy resources, and contribution to power system stability.

Rojan Bhattarai (Member, IEEE) received the B.E. degree in electrical engineering from the Institute of Engineering, Pulchowk Campus, Tribhuvan University, Kirtipur, Nepal, in 2012 and the Ph.D. degree in electrical engineering from the University of North Carolina at Charlotte, Charlotte, NC, USA, in 2018.

Since then he has been working as a Postdoctoral Intern with Argonne National Laboratory, Lemont, IL, USA. His current research interests include distributed energy systems modeling, and control and stability studies of the renewable integrated power grid.

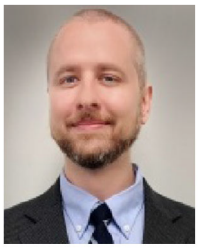

Michael Smith (Member, IEEE) received the B.S. degree in mechanical engineering technology, the M.S. degree in mechanical engineering , the M.S. degree in electrical engineering, and the Ph.D. degree in electrical engineering from the University of North Carolina at Charlotte, Charlotte, NC, USA, in 2005, 2008, 2012, and 2015, respectively.

He is currently an Assistant Professor with the Department of Engineering Technology and Construction Management (within the William States Lee College of Engineering), University of North Carolina at Charlotte. His background includes instrumentation-based process control, data-driven decision making, and software development, with more than 10 years of industrial experience in the energy industry. His research interests include real-time process modeling, stability and control, adaptive control, process automation and optimization, data analytics, applied energy, and electromechanical systems.

Sukumar Kamalasadan (Senior Member, IEEE) received the B. Tech. degree in electrical engineering and electronics engineering from the University of Calicut, Malappuram, India, in 1991, the M. Eng. degree in electrical power systems management from the Asian Institute of Technology, Bangkok, Thailand, in 1999, and the Ph.D. degree in electrical engineering from the University of Toledo, Toledo, OH, USA, in 2004. He is currently working as a Professor with the Department of Electrical and Computer Engineering, University of North Carolina at Charlotte, Charlotte, NC, USA. His research interests include intelligent and autonomous control, power systems dynamics, stability and control, smart grid, microgrid, and real-time optimization and control of power system.

Dr. Kamalasadan has won several awards including the NSF CAREER Award and IEEE Best Paper Award.